IL NUOVO CIMENTO Vol. 35 C, N. 6 Novembre-Dicembre 2012
DOI 10.1393/ncc/i2012-11359-5

Colloquia: LaThuile12

QCD results using jets and photons in ATLAS

D. López Mateos on behalf of the ATLAS Collaboration
Harvard University - Cambridge, MA 02138, USA

ricevuto il 7 Settembre 2012

Summary. — Measurements of jet and photon production performed with data collected during 2010 with the ATLAS detector at the LHC are surveyed. They are compared to leading-order and next-to-leading-order calculations, providing a breadth of tests of QCD at a new energy regime. Agreement is generally found with the most sophisticated calculations, except in regions of phase space where the calculations are expected to reach certain limitations. For those observables for which they are available, next-to-leading-order calculations matched to parton showers are shown to exhibit a large dependence on the choice of parton shower tune, comparable in size to the estimated uncertainties of the perturbative calculations.

PACS 12.38.Qk – Quantum chromodynamics: Experimental tests.
PACS 13.85.Qk – Inclusive production with identified leptons, photons or other non-hadronic particles.
PACS 13.87.-a – Jets in large-Q^2 scattering.

1. – Introduction

The study of the production of jets and photons in proton-proton collisions encompasses a wide variety of key observables in high-energy physics. Photon and jet production can be used to measure the strong coupling constant, obtain information about the proton and photon structures, and provide constraints and develop tools for searches of physics beyond the Standard Model. In what follows, some of the measurements of photon and jet production performed up to date with the ATLAS detector at the LHC are shown and discussed, as well as comparisons to a variety of perturbative QCD calculations combined with models of non-perturbative effects. Photon and jet reconstruction are also discussed, since they constitute a large component of the experimental uncertainties in the measurements presented.

2. – Photon and jet reconstruction and performance

The ATLAS calorimeters are used primarily in the reconstruction and identification of photons and jets [1]. A liquid-argon/lead electromagnetic (EM) calorimeter with fine

segmentation in pseudorapidity (η) and ϕ, and additional segmentation along the direction of the shower development, covers the pseudorapidity range of $|\eta| < 3.2$. Hadronic calorimeters, built using scintillating tiles and iron for $|\eta| < 1.7$ and liquid argon and copper in the end-cap ($1.5 < |\eta| < 3.2$), complement the EM calorimeter. Forward calorimeters extend the coverage to $|\eta| = 4.9$, and are used only for jet reconstruction in this document.

2˙1. *Photon reconstruction and identification.* – Photons are reconstructed using the full longitudinal segmentation of the EM calorimeter. Photon identification is performed using properties of the longitudinal and transverse shower development, and includes the rejection of showers that leak into the hadronic calorimeter. For the tight identification used in the measurements presented, cuts are performed on nine shower shape variables. Observed differences between these variables in data and Monte Carlo simulation are considered in the estimation of the systematic uncertainties in purity and efficiency measurements. An additional isolation cut is performed on the energy deposited in a cone of radius 0.4 in $[\eta, \phi]$ around the photon candidate to reduce fakes in the analyses discussed in this document.

One of the dominant systematic uncertainties in measurements with photons arises from uncertainties in the measurement of photon purities. One of the methods used for this measurement is illustrated at the top of fig. 1a. The measurement exploits the isolation cut and the removal of some of the tight selection requirements to build three control regions with enhanced background contributions. The estimate of the number of background events in the signal region is obtained as the ratio of events in regions C to D, normalized by the number of background events found in region B. The method includes corrections for signal contamination in the control regions. The bottom of the figure represents an extension of the method needed for diphoton measurements, where the purity of the subleading photon is estimated with a similar approach when the leading photon falls in the signal region.

Measured purities have been cross-checked with several methods, including one illustrated in fig. 1b, where the isolation variable across regions A and B is considered as a continuous variable and a template fit is performed to obtain the background and signal contributions. The background templates are obtained in regions C and D. Results are consistent for all methods used.

Systematic uncertainties in the purity estimates arise from the degree of correlations between the different regions, differences in the shower shapes between data and Monte Carlo simulations, and definition of the C and D regions, among other less significant effects. The purity estimate obtained for one of the prompt photon measurements presented is shown in fig. 1c with its associated systematic uncertainties.

2˙2. *Jet reconstruction and systematic uncertainties in the jet energy scale.* – Calorimeter jets are reconstructed using the anti-k_t jet algorithm [4] with resolution parameters $R = 0.4, 0.6$ and a four-momentum recombination scheme. Jets are constructed with topological clusters at the electromagnetic scale and calibrated with a scheme designed to bring the calorimeter jet energy to the energy of the truth particle jets on average [5]. Truth particle jets are reconstructed using the same algorithm as calorimeter jets but using as input stable particles with a lifetime longer than 10 ps after hadronization.

Systematic uncertainties in the jet energy scale are estimated propagating to jets measurements of the response of single particles. The measurements have been performed

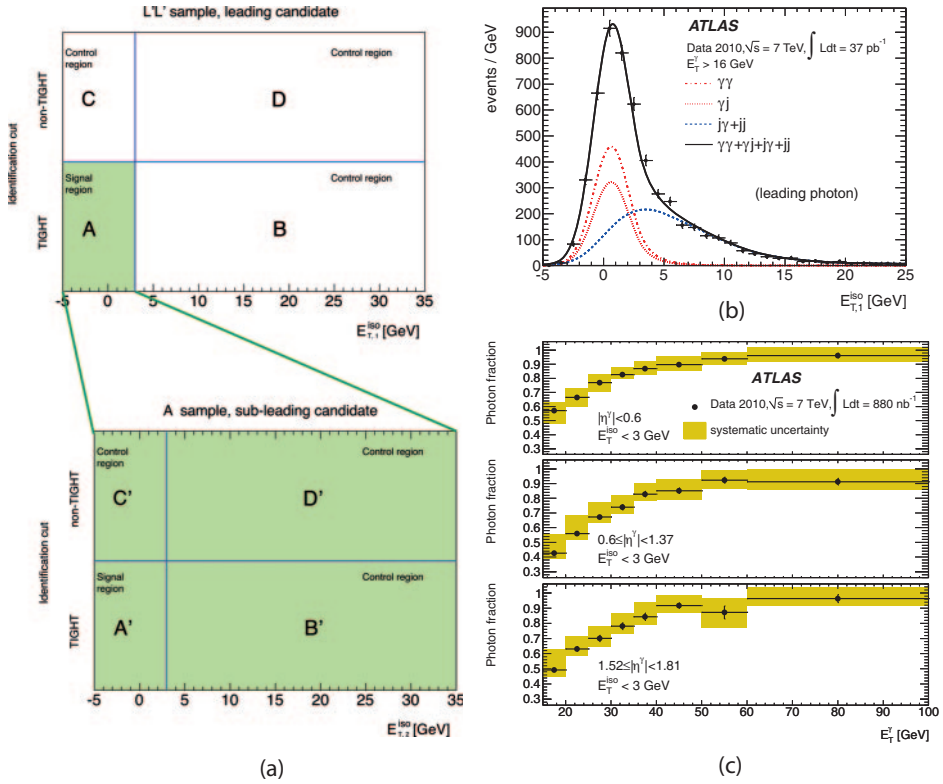

Fig. 1. – (a): Illustration of control regions built to estimate the purity of the photon selection in the diphoton analysis [2]. (b): Template fit to the photon isolation in the tight region for the diphoton cross section measurement [2]. Note that the isolation energy can be negative due to detector resolution effects. (c): Measured purities for different photon rapidity regions as a function of the photon p_{T} for the prompt photon production measurement [3]. Systematic uncertainties in the purity are shown as shaded error bands.

using test beams [6] and collision data [7]. The response of certain neutral particles has not been measured, and a conservative systematic uncertainty is estimated using different models of the hadronic shower in the detector simulation [5]. Additional systematic uncertainties are considered to account for fragmentation effects in the particle p_{T} spectrum inside the jet, the limited knowledge of the dead material in the final detector configuration, and the impact of threshold effects for particles showering in the dense environment inside a jet. The total systematic uncertainty and these individual components are shown in fig. 2 (left).

Since the single particle analysis can only be performed in the central region of the detector that was represented in the test beam measurements, an additional systematic uncertainty is added to account for differences in the calibration as a function of η. This uncertainty is estimated *in situ* using the p_{T} balance of jets in a dijet system, and it is dominated by limitations in the *in situ* method that make it sensitive to the modeling of the physics in dijet events. This is illustrated in fig. 2 (right), where different models of the underlying physics are represented by different Monte Carlo simulations.

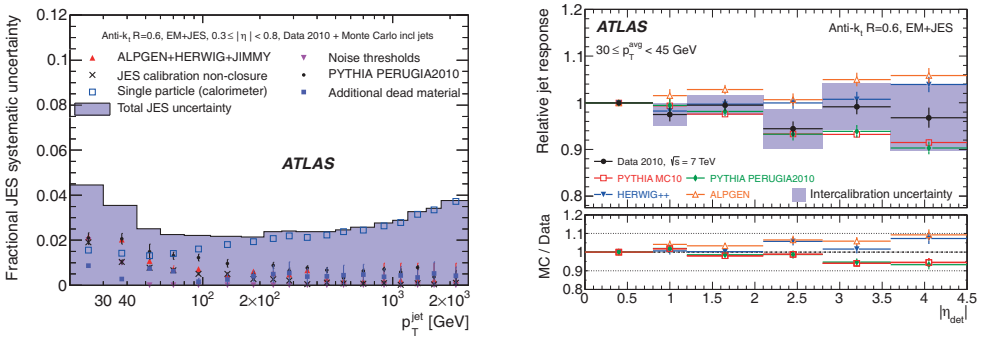

Fig. 2. – Left: Systematic uncertainties in the jet energy scale as a function of jet p_{T} for jets in the barrel. Right: Relative response of jets measured using dijet p_{T} balance (solid markers) and results obtained with different Monte Carlo simulations (open markers). The resulting η-dependent systematic uncertainty is shown as a shaded error band around the data points [5].

3. – Benchmark measurements

Photon and diphoton production measurements, as well as inclusive jet and dijet production measurements, have been performed at lower energies in a variety of colliders, and constitute the basic, yet insightful, building blocks of the jet and photon physics program with the ATLAS detector.

3˙1. *Prompt photon and photon+jet production measurements*. – Figure 3 (left) shows a measurement of the differential cross section for isolated photon production as a function of photon E_{T}. Two measurements are shown, one covering the low-E_{T} region, performed with early data, and another one performed with the full 2010 dataset. Only

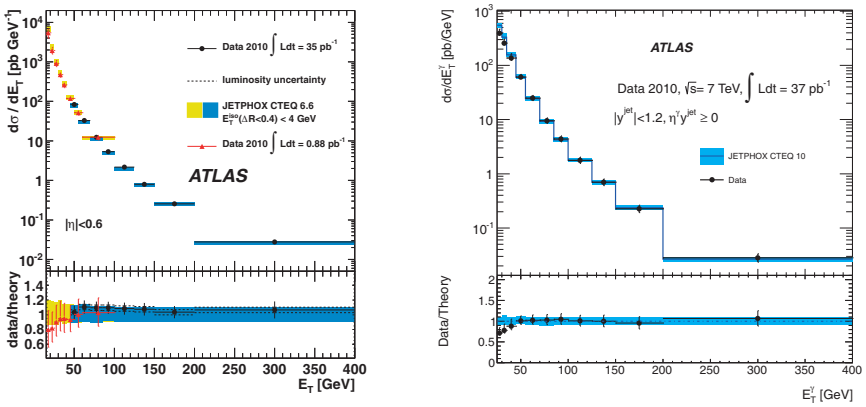

Fig. 3. – Left: Prompt photon production cross section as a function of photon E_{T} for isolated photons falling in the central region of the detector ($|\eta| < 0.6$) [8]. Right: Photon production cross section for photons produced in association with a jet in the same rapidity hemisphere and when the jet falls in the central region of the detector ($|y| < 1.2$). Data results are shown as solid points and the next-to-leading-order calculation and associated systematic uncertainties are shown as shaded error bands [9].

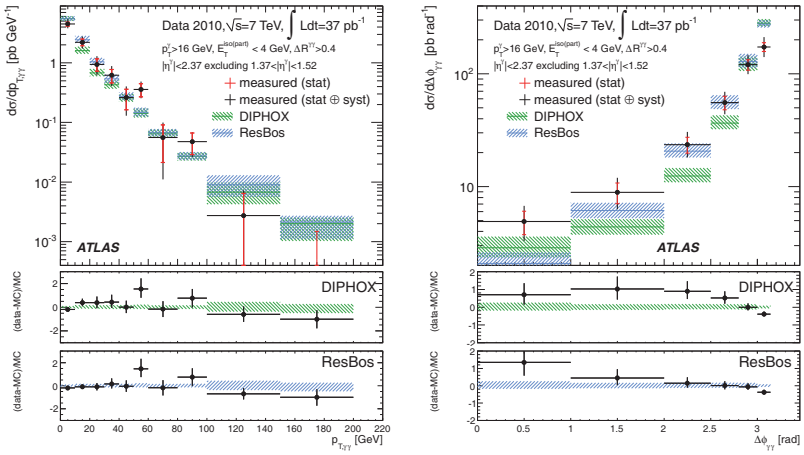

Fig. 4. – Measured differential cross section for diphoton production as a function of p_{T} of the diphoton system (left) and opening angle in ϕ of the diphoton system (right) for isolated photons compared to a next-to-leading-order calculation and a calculation including resummation of next-to-next-to-leading logarithms [2].

the measurement in the central rapidity bin is shown. The result is compared to a next-to-leading-order calculation and shows differences at low E_{T} which are, however, consistent with the calculation within systematic uncertainties.

In hadron colliders, prompt photon production happens primarily in association with a jet. Explicit study of the correlations between the photon and the jet allows for further understanding of the details of parameters entering theoretical calculations such as the proton structure functions. Figure 3 (right) shows a measurement of the differential cross section for isolated photon production as a function of photon E_{T} when the photon is produced in the same rapidity hemisphere as an associated jet with $p_{\mathrm{T}} > 20\,\mathrm{GeV}$. Similar agreement with theory as in the prompt photon production measurement is found, and no significant dependence on the hemisphere correlations has been observed.

3˙2. *Diphoton production measurement.* – Figure 4 shows differential cross section measurements as a function of diphoton p_{T} (left) and opening angle in ϕ between the photons (right) for isolated photons. Comparisons are performed to a next-to-leading order calculation (DIPHOX) and a next-to-leading-order calculation with a parameterized treatment of photon fragmentation and resummation of next-to-next-to-leading logarithms (ResBos). The differential cross section as a function of p_{T} is well described by both calculations, as well as the differential cross section as a function of the invariant mass (not shown). Both calculations, however, fail to predict a $\Delta\phi$ distribution that is less strongly peaked for back-to-back configurations. The prediction provided by ResBos is closer to the data, as expected, due to the impact of large logarithms on event shape variables.

3˙3. *Inclusive and dijet production measurements.* – Figure 5 shows the ratio of the measured inclusive jet cross section to a baseline next-to-leading-order calculation corrected for non-perturbative effects. The ratios of different predictions of a next-to-leading-order calculation matched with different parton showers to the baseline calculation

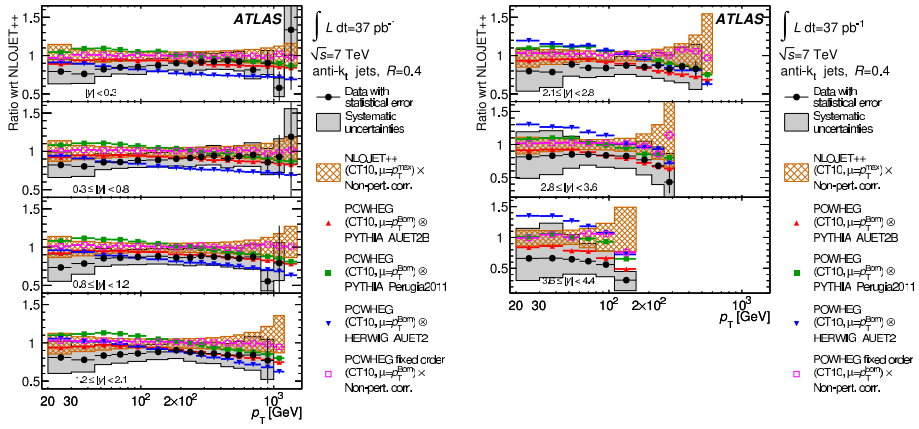

Fig. 5. – Ratio of measured inclusive jet cross section to next-to-leading-order calculation using NLOJet++ and the CT10 parton distribution functions (solid points). Different rapidity bins are shown and jets built with $R = 0.4$ are used. The shaded area around the data points represent the systematic uncertainty in the measurement. The hatched area around 1 represents the systematic uncertainty in the next-to-leading-order calculation. The other markers represent the next-to-leading-order calculation matched to parton showers implemented in POWHEG with different tunes and implementations [10].

are also shown. The measurement agrees within systematic uncertainties with the fixed-order prediction, except in the highest p_{T} and rapidity bins. The measurement is, however, systematically lower than the prediction. This effect has been shown to become significantly smaller when using jets built with $R = 0.6$ [10]. The predictions from calculations with different parton showers show a large spread, of size comparable to that of the uncertainties in the perturbative calculation.

Figure 6 presents the dijet cross section measurement as a function of the dijet invariant mass compared to theoretical calculations as in fig 5. The measurement is binned in y^*, the rapidity of the dijet system in its center of mass. The results show similar features to those observed in the inclusive jet measurement.

4. – Further measurements and insight into QCD

The availability of a higher center-of-mass energy at the LHC, and new theoretical tools allows for additional measurements that provide further insight into QCD. A small selection of such measurements is discussed in what follows.

4·1. *b-jet cross section measurements.* – Figure 7 shows the ratio of the measured inclusive b-jet cross section to two next-to-leading-order predictions matched to parton showers. Agreement is found between data and the prediction obtained with POWHEG, and it has been shown to not depend on whether POWHEG is interfaced to Pythia or Herwig/Jimmy. A significant disagreement is, however, found in comparisons with MC@NLO, demonstrating the importance of the details of the matching of the next-to-leading-order calculations to the parton shower.

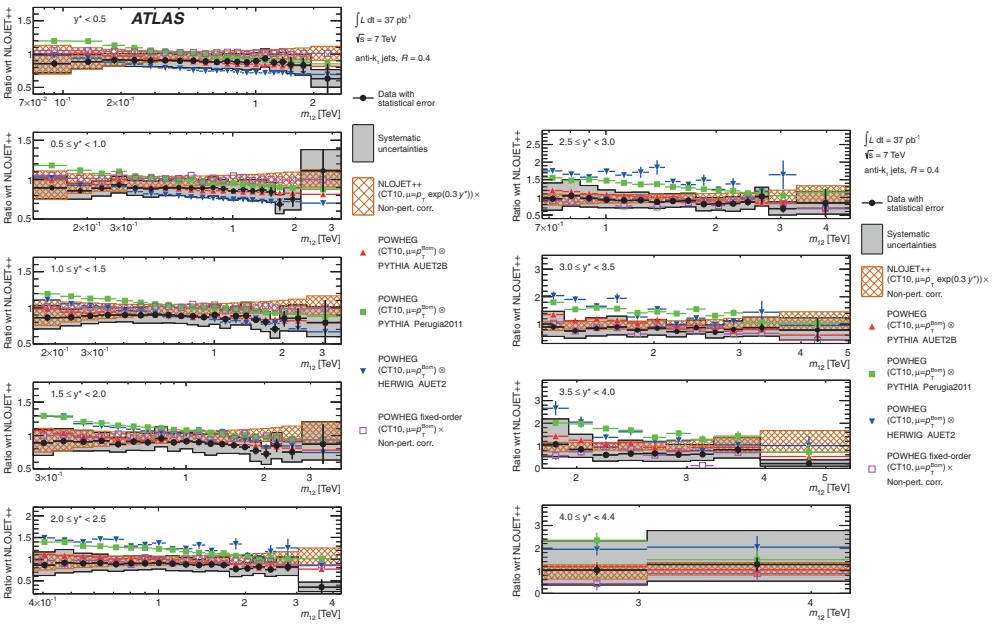

Fig. 6. – Ratio of measured dijet cross section to next-to-leading-order calculation using NLOJet++ and the CT10 parton distribution functions (solid points). Different y^* bins are shown and jets built with $R = 0.4$ are used. The different curves shown are as in fig. 5 [10].

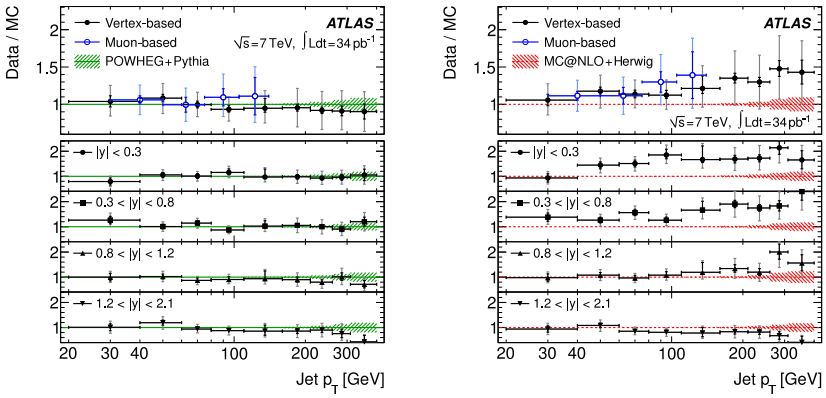

Fig. 7. – Ratio of measured inclusive b-jet cross section to next-to-leading-order calculations interfaced to parton showers. Measured cross sections are shown as calculated through fits to vertex properties and to properties of a muon associated to the jet when enough events were available. Theory predictions correspond to those obtained with POWHEG+Pythia (left) and MC@NLO+Herwig/Jimmy (right). Results are shown in the full rapidity range studied (top figures) and for different rapidity ranges. Statistical uncertainties are shown as dark error bars and the total uncertainty as lighter error bands [11]. The shaded band around 1 represents the statistical uncertainties in the theoretical calculation, scale and proton structure function uncertainties being small compared to the uncertainties in the measurement.

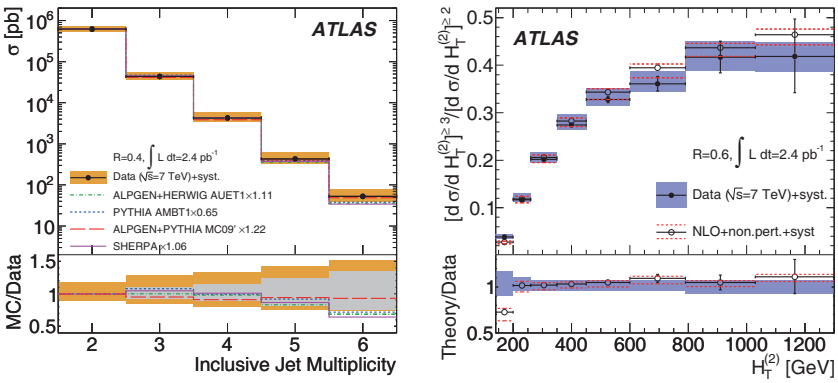

Fig. 8. – Left: Measured inclusive jet multiplicity cross section compared to different leading-order calculations, normalized to the inclusive 2-jet cross section. The systematic uncertainty in the measurement is shown as a shaded error band around the data. The ratios of the different Monte Carlo simulations to the data are shown on the bottom plot. The light-shaded band on the bottom plot shows the systematic uncertainties in the measurement of the shape of the distribution. Right: Measured ratio of 3-jet to 2-jet cross section as a function of $H_{\mathrm{T}}^{(2)}$ (solid points) compared to a next-to-leading-order calculation (open points) using NLOJet++. The bands around the data represent the systematic uncertainty in the measurement, and the dashed lines around the calculation bracket the systematic uncertainty in the calculation [12].

4·2. *Multijet cross section measurements.* – Figure 8 shows the measurement of the production cross section as a function of the inclusive jet multiplicity and the measurement of the ratio of the 3-jet to 2-jet cross sections as a function of the sum of the p_{T} of the two leading jets ($H_{\mathrm{T}}^{(2)}$). The shape of the inclusive jet multiplicity distribution depends largely on the parton shower tune used, and does not agree with the measurement for the highest multiplicities for most tunes.

The cross section ratio measurement compares well to the next-to-leading-order calculation, except in the lowest bin, where kinematic cuts in the selection are likely to constrain the phase space to regions where the next-to-leading-order calculation reaches its limitations. Systematic uncertainties in the ratio measurement are comparable to theoretical uncertainties in the calculation. Jets built with $R = 0.6$ are used in this comparison. Results using $R = 0.4$ show larger uncertainties in the perturbative calculation [12].

5. – Conclusions and future prospects

Comparisons have been shown for a variety of measurements and next-to-leading-order calculations, including calculations matched to parton showers. Generally, agreement is found between data and the theoretical calculations, and the uncertainties in the measurement are of comparable in size to those in the perturbative calculations. Comparisons with different parton shower tunes interfaced to matrix-element calculations have revealed the importance of the choice of tune when attempting to understand systematic effects in the predictions. Work to understand the differences between the tunes will help future measurements and searches for physics beyond the Standard Model. In addition, new analyses are being performed that will use the current measurements to constrain

the parameters entering QCD calculations and gain the fundamental understanding that will allow for a comprehensive physics program using jet substructure [13].

REFERENCES

[1] ATLAS Collaboration, *JINST*, **3** (2008) S08003.
[2] ATLAS Collaboration, *Phys. Rev. D*, **85** (2012) 012003.
[3] ATLAS Collaboration, *Phys. Rev. D*, **83** (2011) 052005.
[4] Cacciari M., Salam G. P. and Soyez G., *JHEP*, **04** (2008) 063.
[5] ATLAS Collaboration, arXiv:1112.6426; to be published in *Eur. Phys. J. C*.
[6] Aharrouche M. *et al.*, *Nucl. Instrum. Methods A*, **614** (2010) 400.
[7] ATLAS Collaboration, arXiv:1203.1302; to be published in *Eur. Phys. J. C*.
[8] ATLAS Collaboration, *Phys. Lett. B*, **706** (2011) 150.
[9] ATLAS Collaboration, *Phys. Rev. D*, **85** (2012) 092014.
[10] ATLAS Collaboration, *Phys. Rev. D*, **86** (2012) 014022.
[11] ATLAS Collaboration, *Eur. Phys. J. C*, **71** (2011) 1846.
[12] ATLAS Collaboration, *Eur. Phys. J. C*, **71** (2011) 1763.
[13] ATLAS Collaboration, *JHEP*, **05** (2012) 128.